JACS Au
AN OPEN ACCESS JOURNAL OF THE AMERICAN CHEMICAL SOCIETY

pubs.acs.org/jacsau

Article

Topographical Design and Thermal-Induced Organization of Interfacial Water Structure to Regulate the Wetting State of Surfaces

Yi Wang,‡ Weinan Zhao,‡ Mei Han, Jiaxin Xu, Xiaoming Zhou, Wesley Luu, Lian Han, and Kam Chiu Tam*

Cite This: *JACS Au* 2022, 2, 1989–2000

Read Online

ACCESS | Metrics & More | Article Recommendations | Supporting Information

ABSTRACT: Smart surfaces with superhydrophobic/superhydrophilic characteristics can be controlled by external stimuli, such as temperature. These transitions are attributed to the molecular-level conformation of the grafted polymer chains due to the varied interactions at the interface. Here, tunable surfaces were prepared by grafting two well-known thermo-responsive polymers, poly(*N*-isopropylacrylamide) (PNIPAM) and poly(oligoethylene glycol)-methyl ether acrylate ($POEGMA_{188}$) onto micro-pollen particles of uniform morphology and roughness. Direct Raman spectra and thermodynamic analyses revealed that above the lower critical solution temperature, the bonded and free water at the interface partially transformed to intermediate water that disrupted the "water cage" surrounding the hydrophobic groups. The increased amounts of intermediate water produced hydrogen bonding networks that were less ordered around the polymer grafted microparticles, inducing a weaker binding interaction at the interface and a lower tendency to wet the surface. Combining the roughness factor, the bulk surface assembled by distinct polymer-grafted-pollen microparticles (PNIPAM or $POEGMA_{188}$) could undergo a different wettability transition for liquid under air, water, and oil. This work identifies new perspectives on the interfacial water structure variation at a multiple length scale, which contributed to the temperature-dependent surface wettability transition. It offers inspiration for the application of thermo-responsive surface to liquid-gated multiphase separation, water purification and harvesting, biomedical devices, and printing.

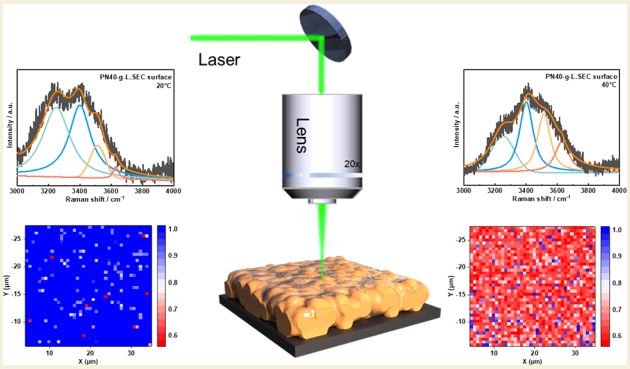

KEYWORDS: *thermo-responsive surface, surface wettability transition, interfacial water structure, Raman spectroscopy, poly(N-isopropylacrylamide), poly(oligoethylene glycol)methyl ether acrylate*

INTRODUCTION

Thermo-responsive polymer composites and coatings are a class of smart materials that find broad applications in wearable devices and drug delivery due to their switchable and programmable properties.[1] Particularly, the thermo-responsive behavior of polymers provides an effective strategy to design systems with tunable properties. These systems possess interesting physics associated with the conformational transition triggered by temperature that is still not completely understood.

Thus far, PNIPAM and $POEGMA_{188}$ are the two most widely studied thermo-responsive polymers due to their sharp thermal transition and their LCSTs being close to the body temperature. These transitions have been studied using many different techniques,[2,3] such as laser light scattering, fluorescence spectroscopy, turbidimetry, differential scanning calorimetry (DSC), infrared spectroscopy, nuclear magnetic resonance, and Raman spectroscopy, to understand the phase transition of thermo-responsive polymers in aqueous solutions. Two main conclusions were derived from these experiments, the coil-to-globule state of polymer and associated functional group transition.[4] For thermal-responsive polymers grafted to bulk surfaces, the current understanding is that the wettability transition near the LCST depended on the exposed functional groups.[5] Nevertheless, the studies consistently claimed that the functionalized surface groups could only affect the water molecule directly in contact with or extremely close to (normally 1−2 nm) the interface.[6] Thus, fundamental understanding on how such a short-range interaction that influences the macroscopic wettability transition is necessary for the manipulation of the bulk surface wettability.

Lycopodium sporopollenin extine shell (L.SEC) microparticles have gained increasing attention for applications, such as drug carriers,[7] sensors, and soft robotics.[8] Owing to the

Received: May 6, 2022
Revised: August 5, 2022
Accepted: August 8, 2022
Published: August 18, 2022

https://doi.org/10.1021/jacsau.2c00273
JACS Au 2022, 2, 1989−2000

unique morphology and versatile physical and chemical characteristics, L.SEC particles could be a good substrate for grafting thermo-responsive polymer brushes that offer us a flexible platform to investigate the polymer−water interactions. From the microscopic perspective, the grafting of thermo-responsive polymer brushes on rigid particles can enhance the structural stability that minimizes the aggregation of the polymer chains. In addition, the surface functionality of the L.SEC offers sufficient amounts of chemical reactive sites (hydroxyl groups) for the grafting of the polymer chains. Most importantly, these microparticles are naturally produced in plants, and hence they are renewable and abundant and are a good source of materials for a variety of applications.

Herein, we prepared thermally induced surfaces by grafting two representative thermo-responsive polymers, poly(*N*-isopropylacrylamide) (PNIPAM) and poly(oligoethylene glycol)-methyl ether acrylate ($POEGMA_{188}$) onto pollen microparticles with a uniform morphology and roughness to investigate the water−surface interaction at different length scales. We demonstrated that the temperature-dependent interfacial properties of the polymer grafted L.SEC particles are associated with the interaction between interfacial water film and apolar/polar groups of the polymer brushes, as revealed by *in-situ* Raman spectra and thermodynamic analysis. Additional rheological measurements suggested that the transformation of the interfacial water structure near the polymer brushes can be amplified on each polymer grafted L.SEC particle due to the rearrangement of the hydrogen bonding network during the LCST transitions. The formation of the distinct hydrogen bonding network at the microscale on rough surfaces can effectively induce the bulk surface wettability transition, which can be elucidated by surface free energy calculations, 3D confocal microscopy imaging, and liquid contact angles under different environmental conditions. This study provides fundamental insight and understanding into the relationship between the interfacial water structure and surface wettability transition. Furthermore, these findings offer a new route to design thermo-responsive colloids and surfaces (or other stimuli-responsive systems) for a wide range of applications, such as liquid-gated multiphase separation,[9] water purification and harvesting,[10−12] biomedical devices,[13] and printing.[14]

MATERIALS AND METHODS

Materials

Lycopodium clavatum pollen (Flinn Scientific Canada Inc.), Lotus pollen, *N*-Isopropylacrylamide, di(ethylene glycol) methyl ether methacrylate, cerium(IV) ammonium nitrate, potassium hydroxide, phosphoric acid, acetone, ethanol, and rhodamine B were used as received from Sigma-Aldrich. All chemicals were used without additional purification, unless stated otherwise. Milli-Q water (resistivity of 18.2 MΩ cm) was used to prepare the aqueous dispersions.

Preparation of Lycopodium Sporopollenin Extine Shell (L.SEC)

Natural *Lycopodium clavatum* pollen grains were defatted to remove lips and intine materials yielding indestructible, ultra-tough, defatted pollen microcapsules. For this purpose, *Lycopodium clavatum* pollen granules (50 g) were refluxed in acetone (300 mL) for 3 h in a round-bottom flask under magnetic stirring (50 °C, 350 rpm). The defatted pollen grains were recovered via vacuum filtration for intine material extraction. This process involves pollen shell extraction and subsequent incubation in an alkaline medium, where the defatted pollen was treated with 10 wt% potassium hydroxide (KOH) at 80 °C and stirred for 2 h to remove the internal cytoplasmic content. KOH-treated spores were then subjected to acidolysis by stirring them in 200 mL of 85 wt% phosphoric acid (H_3PO_4) at 60 °C for 3 h. After the acid treatment, the spore solution was cooled, and washed extensively with water, acetone, and ethanol, and filtered. Finally, H_3PO_4-treated spores were dried at 60 °C for 24 h in an oven, and the weight of the final dried spores was measured. L.SEC samples after each chemical treatment step were recovered for analysis. All the spores were stored at room temperature before their use in subsequent chemical modifications.

Preparation of Thermal-Responsive L.SEC-Based Superhydrophobic System

First, 100 mL of L.SEC (0.1 g) aqueous dispersion was mixed with 1.0 mL 70 wt % HNO_3 in a three-neck flask under magnetic stirring and degassed with nitrogen flow. The reaction was allowed to proceed under stirring in an ice bath for 30 min before the polymer grafting. Next, cerium(IV) ammonium nitrate (CAN) (0.05 g 0.10 mmol) was added to the reaction flask forming radical sites on the hydroxyl groups on L.SEC through the reduction of ceric ions. A NIPAM monomer (1.13 g, 10.0 mmol) was introduced to initiate the polymerization, and the solution was kept in an ice bath under slow magnetic stirring for a fixed time period (ranging from 1 to 2, 3, 4, and 6 h). Finally, the product was dialyzed against deionized water until the measured water conductivity remained constant. The reaction was repeated with various amounts of CAN- and NIPAM-grafted moieties. The as-prepared PNIPAM modified L.SEC microparticles were designated as PNm-g-L.SEC where *m* corresponds to the monomer mass ranging from 5 to 10, 20, and 40 mmol (initiator/monomer ratio-*m* is constant). For the polymerization of $POEGMA_{188}$ on L.SEC, an $OEGMA_{188}$ monomer (1.88 g, 10.0 mmol) was introduced to initiate the polymerization (*m*: 2, 5, 10, 20, 40 mmol) and the solution was kept in an ice bath under slow magnetic stirring for a fixed time period. These $POEGMA_{188}$-modified L.SEC microparticles are denoted as POm-g-L.SEC, where *m* corresponds to the monomer mass ranging from 5 to 10, 20, and 40 mmol.

Preparation of Thermal-Responsive L.SEC-Based Superhydrophobic Surface

The L.SEC-based superwettable surfaces were constructed via the immobilization of polymer-L.SEC onto an aluminum sheet. We sprayed the L.SEC powder on the aluminum sheet coated with an adhesive glue, where the surfaces were uniformly prepared, and the coating thickness was manipulated by adjusting the concentration of the formulation. The coated surface was vacuum dried, after which they were subjected to further analysis.

Characterization

The water/oil static and dynamic contact angle measurements were performed using the OCA 15 (Dataphysics). To measure the static contact angle, a sessile drop (5 μL) was dispensed onto the test surface with an auto-dosing system equipped with a 500 μL needle, and a side-view image was captured with the camera when the droplet was stabilized. To obtain an accurate value of the static contact angles, the captured image was further analyzed with the Image J analysis software. L.SECs were visualized and examined from optical microscopic images and videos captured using the Nikon LV ND microscope or Photron SA5 high-speed camera. The particle size was measured using a particle size analyzer (Anton Paar 1190) and Nano Zetasizer (Malvern ZS90) with a temperature control system. The thermal responsive characteristics were evaluated by performing turbidimetric measurements on the Varian (Cary 100 Bio) UV−vis spectrometer equipped with a temperature controller and micro-differential scanning calorimetry (DSC). Raman spectroscopy was conducted on a LabRam HR800 confocal Raman microscope (HORIBA JobinYvon) with ×50 and ×20 objectives (excitation at 532 nm). The surface topography was characterized via the scanning electron microscopy (SEM) and confocal optical microscopy (Olympus LEXT ols5000). Elemental analyses were conducted using energy dispersive X-ray spectroscopy (EDS-SEM) and X-ray photoelectron spectroscopy (XPS) (Escalab 250XI, Thermo Scientific, USA). The rheological properties of the concentrated suspension were characterized in a Malvern Kinexus Ultra + rheometer with the cylindrical measuring system and a solvent trap to

https://doi.org/10.1021/jacsau.2c00273
JACS Au 2022, 2, 1989−2000

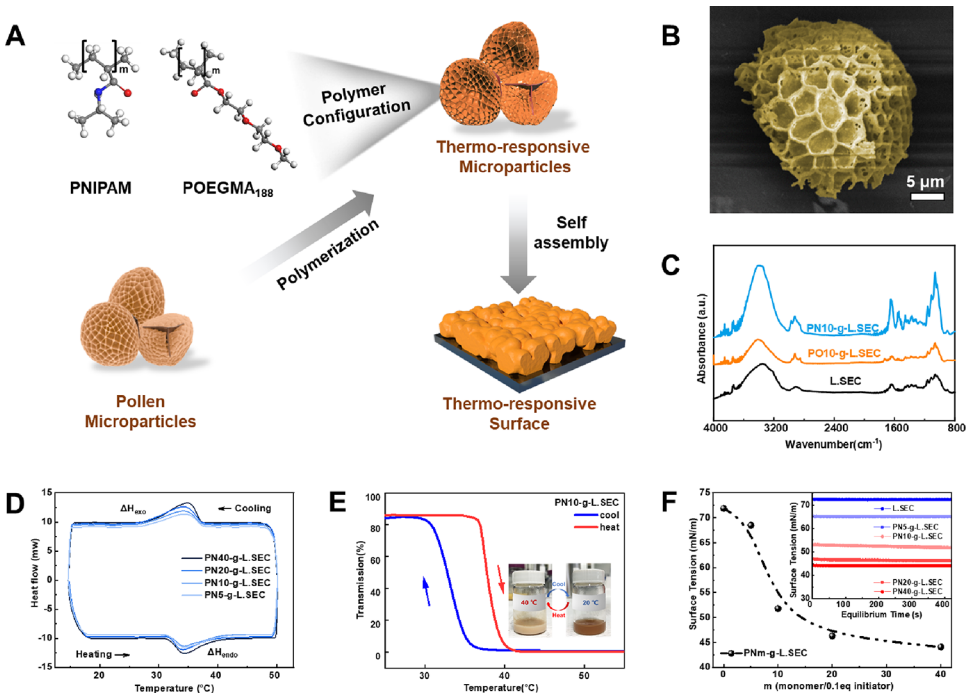

Figure 1. (A) Schematic of preparation of thermo-responsive L.SEC particles and surfaces by grafting PNIPAM and $POEGMA_{188}$. (B) SEM images of pristine L.SEC. (C) FT-IR spectra of PN10-g-L.SEC, PO10-g-L.SEC, and L.SEC. (D) DSC measurement on PNm-g-L.SEC ranging the temperature from 15 to 50 °C with a scanning rate of 1 °C/min. (E) Turbidity change of PN10-g-L.SEC aqueous solution measured by UV−vis spectrophotometry. (F) Surface tension of PNm-g-L.SEC detected by a tensiometer.

prevent water evaporation. The measured confocal laser scanning confocal microscopic (CLSM) (Zeiss LSM 510-Meta) image was shaped into a 3D image using ZEN 2009 analysis. The observation magnification was 40×/1.3 Water DIC, and an immersion objective lens was used, with the immersion medium being water.

RESULTS AND DISCUSSION

Polymer-L.SEC Microparticles

The thermo-responsive L.SEC microparticles were synthesized by performing cerium nitrate (CAN) free radical polymerization of *N*-isopropylacrylamide (NIPAM) and (oligoethylene glycol) methyl ether acrylate ($OEGMA_{188}$) in water (Figure 1A). First, L.SEC microparticles with a tripartite structure decorated with honeycomb-like microridges (1−2 μm height and 200 nm width) on the external surface with a uniform shape of 29.02 μm were prepared via the KOH extraction process (Figure S1).[8] Notably, the hollow L.SEC with a large surface area offered a facile method to control the external polymer layer architecture, consisting of polymer grafting density and chain length.[15] We manipulated these two factors by changing the monomer/initiator mass ratio and polymerization time. L.SECs were designated as PNm-g-L.SEC and POm-g-L.SEC, where *m* corresponds to the molar ratio of the monomer to 0.1 equiv of the initiator varying in 5, 10, 20, and 40 mmol. A brown L.SEC powder was obtained and characterized by scanning electron microscopy (SEM), showing the surface morphology of PNm-g-L.SEC and POm-g-L.SEC with a higher roughness nanostructure on micro-ridges owing to the polymer grafted canopy compared to pristine L.SECs (Figure 1B). Specifically, the architecture of the polymer grafted canopy of PNm-g-L.SEC particles transformed from a sparse to dense structure with a rough nanostructure that increased with the increasing grafting ratio (Figure S2). Moreover, changes in the particle size were strongly associated with the polymer layer thickness as summarized in Table S2. For example, the size of PN-g-L.SEC increased from 30.51 to 31.62 μm as *m* increased from 5 to 40 mmol, corresponding with the epicuticular polymers covering the microridges on the outer surface becoming dense and increasing the thickness from 260.9 to 762.3 nm. POm-g-L.SEC showed a similar structural change as PNm-g-L.SEC. The induced structural and hydrophobicity change of modified L.SECs (PNm-g-L.SEC and POm-g-L.SEC) had a profound impact on the L.SEC-based thermo-responsive surfaces. Fourier transform infrared spectroscopy (FT-IR) further confirmed the successful grafting of PNIPAM and $POEGMA_{188}$ on the extine of L.SEC.[16] The IR spectrum of PN10-g-L.SEC displayed two characteristic peaks that confirmed the presence of amine groups, where the first band at 1650 cm^{-1} is associated with the N-C=O bond, while the absorption peak at 1550 cm^{-1} corresponds to the N−H bonds. The isopropyl groups (IP) were confirmed by the IR spectra over the range of 2500 to 4000 cm^{-1}. The peak at 2970 cm^{-1} was assigned to the antisymmetric and symmetric CH stretch of the methyl groups, while the peaks at around 2850 and 2871 cm^{-1} were derived from the symmetric stretches of CH_2 and CH_3, respectively.[17] As shown in Figure 1C, PO10-g-L.SEC displayed a unique peak on 1740 cm^{-1}, which corresponds to the ester linkage between the methacrylate and oligoethylene glycol side chains of the $POEGMA_{188}$ graft brushes.[4] Further evidence on the successful polymerization of NIPAM and OEGMA from the surface is provided by X-ray photoelectron spectroscopic (XPS) elemental analyses, confirming that this layer contained organic molecules with the expected changes in the ratio of the C−N bond on the PNm-g-L.SEC surface and C−O bond on the POm-g-L.SEC surface. (Figure S3 and Table S1).[18]

With regards to thermal responsive characteristics, the polymer conformational transition endowed the L.SEC with different interactions with water molecules that are dependent

https://doi.org/10.1021/jacsau.2c00273
JACS Au 2022, 2, 1989−2000

on the thermal characteristics, such as the lower critical solution temperature (LCST). The LCST driven by temperature was typically associated with the turbidity change, which could be measured by UV−vis spectrophotometry. Figure 1E reveals the LCST of PN10-g-L.SEC solutions at ∼35.2 °C caused by the hydrophobic effect of the isopropyl groups (IP) and bound water around the amine (−NH) and carbonyl groups (-C=O). In addition, the phase transition of PNm-g-L.SEC was further investigated by differential scanning calorimetry (DSC) over consecutive heating/cooling cycles.[19] The LCST transition of the PNm-g-L.SEC revealed two different thermal processes as shown in Figure 1D, a typical endothermic peak at ∼35.8 °C and an exothermic peak at ∼36.2 °C of PN10-g-L.SEC. These thermal transitions are related to the dehydration of apolar groups (IP) and the interactions between polar groups and water molecules. Below the LCST, the polymer chains are in a random coil conformation, with "water cages" surrounding the IP and water molecules or bonding with the -NH and -C=O groups.[20] At temperatures above the LCST, the entropy of the polymer−water system dominated, which was unfavorable for the exothermic formation of hydrogen bonds. Thus, the water cages surrounding the IP groups were disrupted together with the bound water molecules that were released to increase their entropy and the polymers collapsed into a globular state.[21] The phase transition of PN10-g-L.SEC was evident from the inset of Figure 1E determined from the changes in the solution turbidity. PN10-g-L.SEC was well-dispersed in an aqueous solution with an average radius of 31.07 μm at 20 °C, and the solution transformed into a turbid dispersion at 40 °C that became insoluble and the suspension transformed into a brown opaque color, confirming that the grafted PNIPAM chains collapsed and transformed into globules, where the PN10-g-L.SEC possessed an average radius of 30.09 μm (Figure S4).

The polymer chain conformational transition can be traced by the interfacial arrangement of these hydrophobic/hydrophilic segments on PN10-g-L.SEC, which was indicated by changes in the dynamic temperature-dependent surface tension and interfacial behavior between polar/apolar solvents. The dependence of the surface tension with changes in temperatures are displayed in Figure S8D, where γ_{LV} of PN10-g-L.SEC was 52.1 mN m^{-1} at 20 °C decreasing to 38.7 mN m^{-1} at 40 °C. The results demonstrated the predominately strong hydrogen bonding interacting between water molecules with hydrophilic −NH and -C=O groups at low temperature while the exposure of large amounts of hydrophobic IP groups above the LCST reduced the surface tension. The surface tension of PN10-g-L.SEC was thermally responsive and reversible during the heating-and-cooling cycles, while the rearrangement of hydrophobic/hydrophilic groups induced by temperature could also be detected via the time-dependent interfacial tension data (Figure S5).[22] With increasing temperature, the hydrophilic groups formed intramolecular interactions instead of hydrogen bonds with water, where the well-dispersed PN10-g-L.SEC particles in the water phase became hydrophobic and rearranged at the polar/apolar interface. This interfacial behavior of PN10-g-L.SEC resulted in the change of the droplet shape, and the simulated value of the interfacial tension decreased around their LCST, which was consistent with the previous phase transition results.

Moreover, different polymer chain structural arrangements were triggered by temperature, which could be deduced from surface tension. As a result, the equilibrium surface tension (γ_{LV}) of pure L.SEC aqueous solution was about 71.9 mN m^{-1}, which was close to pure water (72.8 mN m^{-1}). With increasing grafting polymer ratio, the amounts of grafted polymer chains on L.SEC increased and γ_{LV} decreased sharply from 68.3 for PN5-g-L.SEC to 44.1 mN m^{-1} for PN40-g-L.SEC(Figure 1F). The results demonstrated the amounts of grafted polymers as deduced from the grafting density and chain length at a low grafting ratio, where the IP groups on the side chain displayed a flat conformation on the pollen surface. However, at a high grafting ratio, the rearrangement of IP groups resulted in an extended and ordered chain conformation, that reduced the water affinity. In addition, the polymer-L.SEC particle morphology could affect the adsorption at the air/water interface. To demonstrate this, we compared the interfacial behaviors between PN10-g-L.SEC microparticles and PNIPAM microgel, where the surface tension variation was recorded. As shown in Figure S7, S8, the surface tension of PN10-g-L.SEC cycled over a smaller range (∼12 °C), and the process was reversible over several cycles, while surface tension of the PNIPAM soft microgel possessed a larger temperature range (∼17−18 °C), and the temperature decreased with each cycle. This is caused by the soft particles deforming and spreading over a larger interfacial area since they possessed a higher adsorption energy compared to rigid particles.[23] When two deformed microgels are forced into close proximity, their size and shape changed irreversibly resulting in a reduced surface tension after several cyclings of between 20 and 40 °C. However, the polymer-L.SEC particles adsorbed at the interface according to the Young−Dupré relationship,[24] endowing them with reversible chemical structural and morphological transition that further ensure a more flexible interaction between water and the stable interparticle interaction compared to the microgel. Therefore, the polymer-L.SEC particles are good candidates for the construction of thermo-responsive surfaces to achieve a tunable and reversible wettability transition.

To compare the influence of molecular structuring on the hydrophobic transition, POm-g-L.SECs were used as reference samples since their polymer chain transitions were different from PNIPAM. The LCST of PO10-g-L.SEC occurred in a reversible phase transition at ∼26.9 °C (Figure S6). Given the mechanism governing the phase transition, the polyethylene glycol (PEG) side chains were solubilized at low temperatures due to the extensive hydrogen bonding between the ether oxygen and water hydrogen atoms. When the temperature was increased beyond its LCST of 26.9 °C, the polymer−polymer interaction became more thermodynamically favorable compared to polymer−water interaction, causing the PEG chains to collapse onto the methacrylate backbone forming an insoluble globule resulting in a turbid solution.[25] The hydrophobic methyl methacrylates (MMA) counterbalanced this hydrophilic character of oligo(ethylene glycol) (OEG) groups leading to a competitive hydrophobic effect. In addition, the LCST temperature of PNm-g-L.SEC was found, similarly to POm-g-L.SEC, to be relatively independent of polymer stereoregularity (Figure S6).

Temperature-Dependent Macroscopic Surface Wettability Transformation

To gain a deep insight into the interactions between water and PNm-g-L.SEC and POm-g-L.SEC, we prepared surfaces with the L.SEC microparticles via the self-assembly of L.SEC microparticles onto a substrate. The combined hierarchical structure reinforced the surface hydrophobic transformation that highlighted the interaction between polymer chain and

https://doi.org/10.1021/jacsau.2c00273
JACS Au 2022, 2, 1989−2000

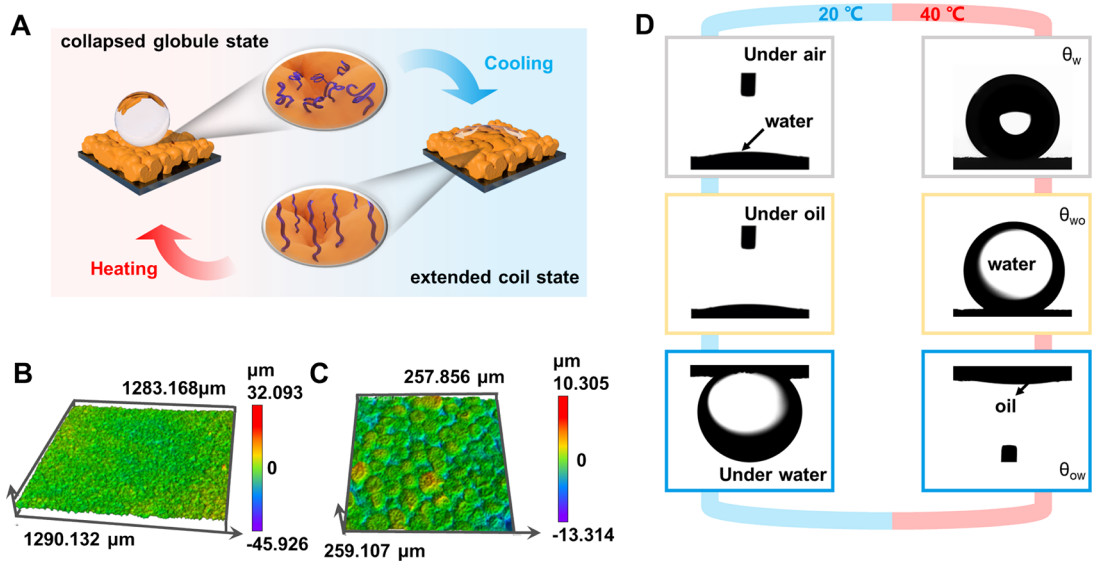

Figure 2. (A) Illustration of surface wettability transition corresponding to the coil-to-globule transition driven by temperature. Surface topography of PN10-g-L.SEC surface measured by laser confocal microscopy: (B) magnification 10×, and(C) magnification 50×. (D) Variation of contact angle on the PN10-g-L.SEC surface under different environmental conditions.

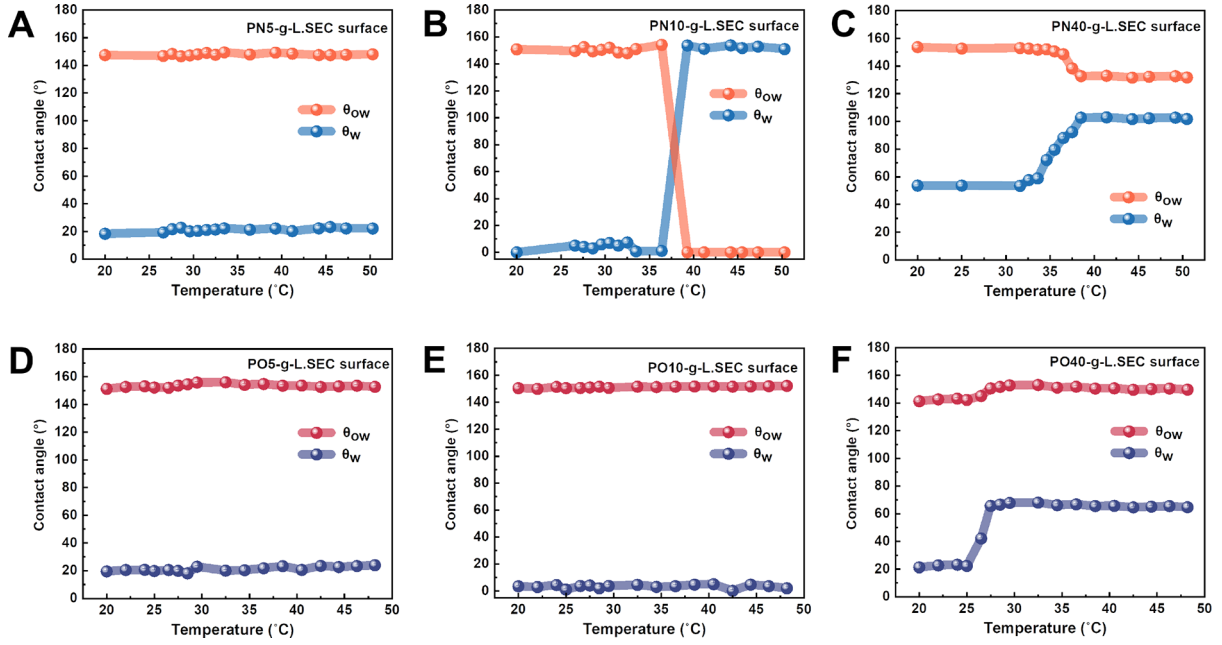

Figure 3. Variation of contact angles including water contact angle under air and oil contact angle under water: (A) PN5-g-L.SEC, (B) PN10-g-L.SEC, (C) PN40-g-L.SEC, (D) PO5-g-L.SEC, (E) PO10-g-L.SEC, and (F) PO40-g-L.SEC.

water molecules, providing a clear and visual picture to demonstrate the process.[26] The surface topography and roughness factor of the L.SEC-based surface were investigated by SEM and laser confocal microscopy. The PN10-g-L.SEC surface possessed a porous network structure with a roughness factor (R_q) of 2.32 μm, where the green−yellow−red regions corresponded to the surface protrusions consisting of assembled L.SEC microparticles and blue regions represented the "valleys" between the protrusions (Figure 2B,C). The convex protrusions comprised self-assembled L.SEC microparticles as indicated by the SEM image (Figure S9). Notably, this surface design strategy could amplify the molecular-level conformational transition for tuning the macroscopic surface characteristics.

The surface wettability behavior is a key parameter to determine the relationship between water and the substrate at the macroscale as characterized by contact angles. Since the surface conformation and structure influenced the water contact angle under air (θ_w), we separated the surfaces into three types for comparison. At a low grafting ratio of polymer (m ∼ 5 mmol), the grafted chain was randomly distributed on the L.SEC surface with low nanoscale roughness, resulting in insufficient functional groups on the outer surface yielding a mild response to temperature changes. As shown in Figure 3A, the PN5-g-L.SEC surface was hydrophilic ($\theta_w \sim 22°$) regardless of the temperature, and the molecular conformation transition at the nanoscale could not alter the surface wettability at the macroscale.[27] A similar surface wettability characteristic was

https://doi.org/10.1021/jacsau.2c00273
JACS Au 2022, 2, 1989−2000

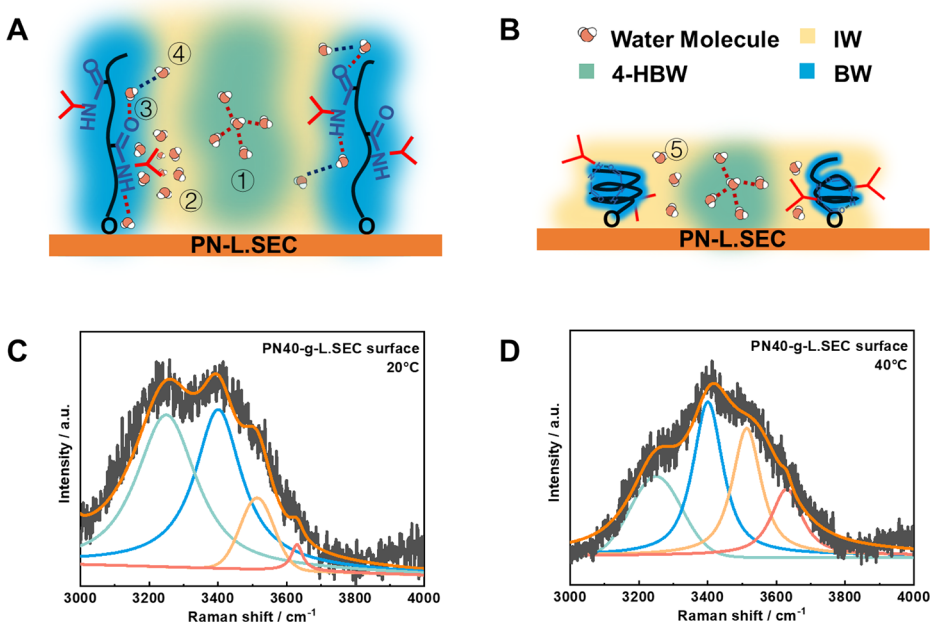

Figure 4. Water structure along the PNIPAM polymer chain: (A) below LCST and (B) above LCST. Proportion of the water ratio measured by Raman spectroscopy: (C) PN40-g-L.SEC surface below LCST and (D) PN40-g-L.SEC surface above LCST.

observed for PO5-g-L.SEC surfaces, (Figure 3D) showing hydrophilicity with a θ_w of 22.4° (20 °C) and 22.1° (40 °C) at low grafting density. Notably, the grafting ratio on L.SEC was a key factor in determining the nano/microstructure of polymer-L.SEC, which further influenced the overall surface topography.

As for PN40-g-L.SEC surface (Figure S9), the surface roughness ($R_q \sim 1.28\ \mu m$) was reduced due to the high grafting ratio of polymer brushes that covered the L.SEC walls and microbridges. The result showed that the high grafting ratio of the polymer altered the hierarchical nano/microstructure, where the increased nano roughness dramatically reduced the micro-roughness. In the case of PN40-g-L.SEC, the surface displayed a hydrophilic/hydrophobic characteristic with a θ_w of 54 ° at 20 °C and 103° at 40 °C (Figure 3C). The reduced microstructure led to the hydrophilic/hydrophobic transition of PN40-g-L.SEC surface, which exhibited a similar trend as the flat polymer surface.[28] Here, with the enhanced nano/microstructure, the surface wettability transformation phenomenon was induced by the molecular structure, orientation, and restructuring of the polymer chain occurring at the water/PNIPAM interface driven by temperature. At low temperatures, the -C=O and -NH groups displayed strong hydrogen bonding with water molecules around the PNIPAM chains that impacted the air/PNIPAM/water interface. When the temperature exceeded the LCST, the polymer chains collapsed and the hydrophilic -C=O and -NH groups interacted via hydrogen bonds while the exposed hydrophobic IP moieties near the surface of the collapsed chains contributed to the hydrophobicity of the PN-g-L.SEC outer surface. In addition, based on the theory of similarity-inter miscibility, hydrophobic groups $_3$) extended to the oil phase and the hydrophilic segments ($-NH_2$, C=O groups) extended toward the water phase. The orientation of the hydrophobic/hydrophilic moieties of the functional groups on the polymer brushes was confirmed by the oil CA under water ($\theta_{o/w}$) and the water CA under oil ($\theta_{w/o}$). PN40-g-L.SEC(20 °C) surface was in a metastable state, possessing under-oil superhydrophobic ($\theta_{wo} \sim 150.5°$) and under-water oleophobic ($\theta_{ow} \sim 151°$) characteristics (Figure S10). Figure 3F shows the thermal switching between hydrophilic and hydrophobic states for the PO40-g-L.SEC surface, where the static θ_w oscillated between 22° at 20 °C and 64° at 40 °C. Although this surface showed a similar thermal wettability transition from hydrophilic to hydrophobic, the molecular structural transformation of POm-g-L.SEC surfaces were different from PNm-g-L.SEC.

To elucidate the surface wettability generated by the hydrophobic/hydrophilic groups, the conformational transition of the polymer brushes on the L.SEC surfaces were analyzed by comparing the total interfacial energy of different wetting states (Figure S13).[29] We compared the total interfacial energies of L.SEC-based surfaces at different temperatures that were completely wetted by either water (E_w) or an arbitrary immiscible oil (hexane) (E_o) or without a fully wetted immiscible water floating on top (E_{wo}).[30] The surface was wetted preferentially by water or oil, and the conformational transition of hydrophobic and hydrophilic moieties on the PNIPAM and $POEGMA_{188}$ triggered by temperature could be estimated. For the PO40-g-L.SEC (20 °C) surface, the comparison of interfacial energy ($E_w < E_o$ but $E_w > E_{wo}$) indicated that the surface would be preferentially wetted by water, forming a stable water−solid interface and displaying hydrophilicity in oil and oleophobicity in water (Table S3). Under this wetting state, the ether oxygens of PEG on the exterior of the collapsed globules bonded with the water molecules. However, the interfacial energy indicated that the water-(PO40-g-L.SEC (40 °C)) surface was thermodynamically unstable, whereas the experimental results showed that the PO40-g-L.SEC(40 °C) surface exhibited an under-oil superhydrophilic ($\theta_{wo} \sim 155.5°$) and under-water superoleophobic ($\theta_{ow} \sim 152.0°$) characteristics. The under-oil superhydrophilic characteristics suggested that the hydrophobic moieties consisting of the methyl groups on the main chain of MMA favored the exterior environment and repelled water, resulting from the enhanced polymer−polymer interactions on the PO40-g-L.SEC (40 °C) surface. In addition, the under-water

https://doi.org/10.1021/jacsau.2c00273
JACS Au 2022, 2, 1989−2000

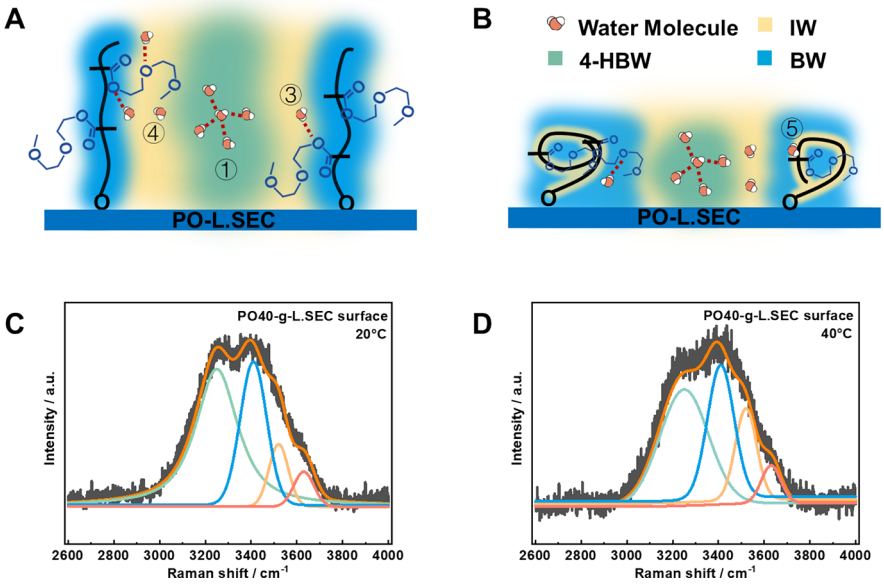

Figure 5. Water structure along the $POEGMA_{188}$ polymer chain: (A) below LCST and (B) above LCST. Proportion of water ratio measured by Raman spectroscopy: (C) PO40-g-L.SEC surface below LCST and (D) PO40-g-L.SEC surface above LCST.

superoleophobic surface suggested that the hydrogen bonding between the side chain of $POEGMA_{188}$ and water persisted in forming a layer of water film that repelled oil, preventing its infusion to the surface. Thus, the molecular conformational transition of the POm-g-L.SEC system associated with the ether oxygens of PEG on the outer surface of the polymer chains bonded with water molecules below the LCST (26.9 °C). Above the LCST, this balance was disrupted and the interaction between the side chain of $POEGMA_{188}$ and water was reduced, resulting in the enhanced polymer−polymer interactions over polymer−water interactions.

Mechanism Investigation of Interfacial Water at Multiple Length Scale and Surface Wettability Transition

Although previous studies suggested that the surface wettability change was induced by the collapsed and extended state of the polymer chains, the associated water structure at the molecular interfaces needed to be determined. To better explore the macroscopic wettability phenomenon at the air/polymer-g-L.SEC/water interface, in situ Raman spectroscopy was used to investigate the changes in the structure and dynamics of water induced by the functional groups on the polymer chains.[31] Here, we presented experimental evidence that revealed a similarity between the structure of water around the hydrophilic/hydrophobic groups and at macroscopic air/PNm-g-L.SEC/water interfaces.

Figure 4 shows a typical Raman spectrum of a fully prewetted and hydrated PN40-g-L.SEC surface over the temperature range from 20 to 40 °C. A broad Raman band extending from 3000 to 4000 cm^{-1} is related to the vibration of hydrogen bonds in water, where the 3250, 3410, 3520, and 3630 cm^{-1} were assigned to different types of water structures. Gaussian fittings of the spectra showed that the O−H stretching band could be resolved into three distinct components, corresponding to three types of O−H stretching vibrations. The low wavenumber component of the 3250 cm^{-1} peak is associated with the vibration of 4-coordinate hydrogen-bonded water (4-HBW), which is attributed to free water with four hydrogen bonds (①) and IP groups surrounded by polyhedral cages composed of tetrahedrally hydrogen-bonded water molecules (②).[20] Whereas, the 3410 cm^{-1} is associated with the in-phase vibrations of water molecules captured by the -C=O or -NH groups (③) of PNIPAM, which is regarded as bound water (BW). The high wavenumber components at 3520 and 3630 cm^{-1} correspond to the stretching of the weak or non-hydrogen bonded water molecules (④⑤), which is regarded as intermediate water (IW), reflecting the hydrophobic disordered water in the hydration shell.[32] Note that the hydration-shell OH band possessed a different shape with changes in temperature ranging from 20 to 40 °C. At 20 °C, the resulting spectra revealed two small dangling (non-hydrogen-bonded) water OH peaks near 3520 and 3630 cm^{-1} as well as two broad overlapping hydrogen-bonded OH features near 3250 and 3410 cm^{-1}. Moreover, at 40 °C, the relative intensity of the Raman band near 3250 cm^{-1} decreased significantly, whereas the high wavenumber components at 3520 and 3630 cm^{-1} showed a dramatic increase. The shift in the spectrum for water structure transformation was attributed to two stages in the polymer chain transition. On one hand, the -C=O or -NH groups formed a strong hydrogen bond around water molecules at low temperatures, which was replaced by intramolecular interaction with each other that weakened the interaction with water molecules above the LCST. On the other hand, IP groups are surrounded by the hydrophobic hydration shells ("water cage") that resemble solid clathrate hydrates below the LCST, which were tetrahedral with fewer weak hydrogen bonds compared to bulk water. When the temperature was increased to 40 °C, the hydration shell transformed dramatically into a less-ordered and weaker H-bonded structure, accompanied by the peaks with a lower intensity of 3250 cm^{-1} and enhanced intensity near 3520 and 3630 cm^{-1}. These results were observed for the PN40-g-L.SEC surface, where the phase transition of PNIPAM chains was accompanied by a water structure transformation.

A better description of the three types of water structures on the PN40-g-L.SEC surface can be described by comparing the proportion of the O−H stretching vibrational band. Analysis of the results in Figure 4C,D revealed that as the temperature was increased from 20 to 40 °C, the proportion of 4-HBW decreased

https://doi.org/10.1021/jacsau.2c00273
JACS Au 2022, 2, 1989−2000

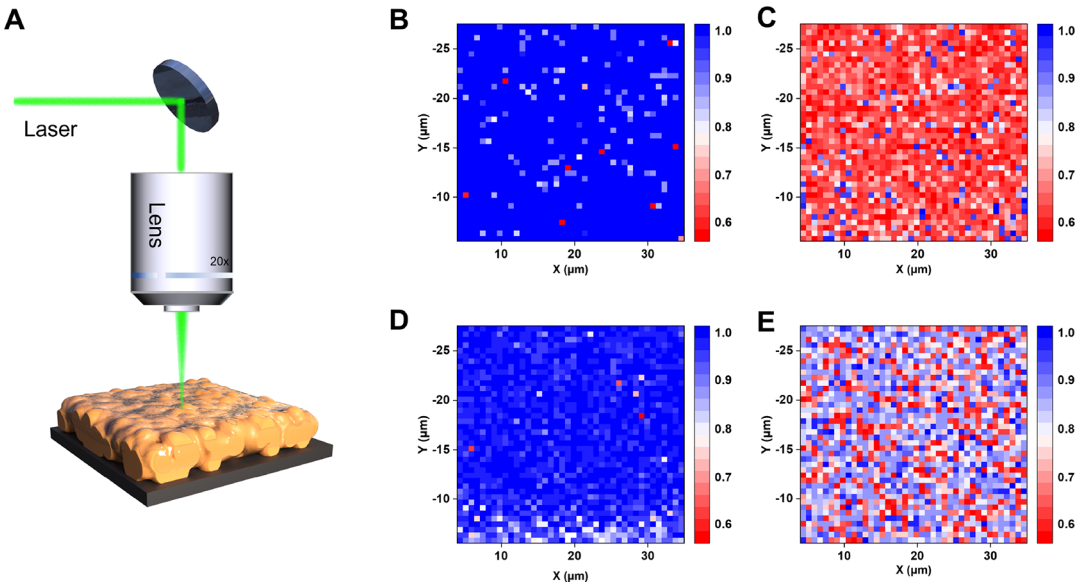

Figure 6. (A) Illustration of temperature-dependent Raman spectroscopy. Water ratio of 4-HBW/BW changing with the temperature detected by Raman mapping (the ratio was measured at each pixel ranging from 0.6 to 1.0 that recorded as red to blue): (B) PN40-g-L.SEC surface at 20 °C, (C) PN40-g-L.SEC surface at 40 °C, (D) PO40-g-L.SEC surface at 20 °C, and (E) PO40-g-L.SEC surface at 40 °C.

from 35.7 ± 1.5 to 21.1 ± 1.3%, BW varied between 36.8 ± 1.4 and 33.0 ± 1.3%, and IW increased from 27.5 ± 1.0 to 45.9 ± 1.2%. Because of the proportion of 4-HBW and BW due to the disruption of the "water cage" surrounding IP groups and dehydration of -C=O and −NH, respectively, we could compare the ratio of 4-HBW/BW to analyze these hydrophilic/hydrophobic orientation and transition around the LCST. Raman mappings on an area of 40 × 40 μm^2 clearly showed the changes of the hydrophilic/hydrophobic orientation and transition on the PN40-g-L.SEC surface at different temperatures (Figure 6). The signal contrast between 20 and 40 °C indicated that the ratio of 4-HBW/BW was higher at 20 °C, revealing that the surface possessed more bound water and the hydrophilic -C=O and −NH groups assembled mainly at the air/PNm-g-L.SEC/water interface. However, the ratio of 4-HBW/BW showed a dramatic drop over the whole area at 40 °C, indicating that the water transformed into a less ordered and weaker hydrogen-bonded structure and the preferred exposure of hydrophobic IP groups rearranged at the interface.

Furthermore, the O−H stretching spectra of the PO40-g-L.SEC surface was selected to investigate the relationship between the water structure and polymer conformation. Theoretical predictions of the conformation of $POEGMA_{188}$ brushes possessed a hydrophobic main chain and a hydrophilic side chain. Figure 5 shows the Raman spectra of PO40-g-L.SEC at 20 and 40 °C, and the proportion of 4-HBW decreased from 35.9 ± 1.3 to 28.7 ± 1.1%, BW varied between 37.8 ± 1.3 and 34.1 ± 1.3%, and IW increased from 26.3 to 37.2 ± 1.0%. Moreover, the ratio of 4-HBW/BW on PO40-g-L.SEC also showed lower fluctuations. These results confirmed that the $POEGMA_{188}$ comprised a strong interaction between C−O and water and a weak hydrophobic hydration shell around the $-CH_3$ of the main chain. Additionally, the signal contrast on Raman mapping of PO40-g-L.SEC revealed that the change in the ratio of 4-HBW/BW was less than the PN40-g-L.SEC surface. Owing to the strong water affinity of C−O groups and the chain structure, the IW layer occurred on the main chain with increasing temperature surrounded by a BW layer (Figure 6). Thus, the hydrophobic hydration shell was different from the "water cage" surrounding IP groups of PNIPAM that did not disappear with increasing temperature, resulting in a lower hydrophobic character of the $-CH_3$ groups.

The water structural variation occurred around the thermo-responsive polymer chains on a molecular level. However, as exhibited by the macroscopic evidence (wettability transformation), such a short-ranged interfacial effect determined the macroscale surface wettability transition when combined with the surface roughness. This could be attributed to the grafting of polymer brushes on the rigid and rough lycopodium pollen, where the water structure variation near the thermo-responsive polymer chain was optimum for the whole pollen particle due to the tendency of the water to maintain the integrity of its hydrogen bond network.[33,34] This phenomenon could be demonstrated by rheological analysis of concentrated pollen suspensions.

The dense suspensions with high volume fraction of particles were prepared near the maximum packing volume fraction, and shear rheological measurements were performed.[35] In general, the rheological properties are extremely sensitive to the interparticle interactions and hydration shell around the particles at the nanoscale. Due to the higher content of 4-coordinate hydrogen-bonded water (4-HBW) and bound water (BW) around the exposed and swollen polymer chain on the PN40-g-L.SEC surface, their ordered hydrogen bond network[36] induced a stable and thick lubricating hydration shell, which kept the particle surfaces separated until a critical load was exceeded resulting in the interpenetration of the brushes below the LCST. This stable lubrication layer would be disrupted at a high shear rate (10^2 s^{-1}), and the hydrodynamic rearrangement of the particles generated larger clusters of aggregated particles, leading to a smooth and reversible viscosity increase (continuous shear thickening in Figure S11).[37] Above the LCST, the interfacial water structure would be substantially altered, where more intermediate water structures were formed around the collapsed polymer chain disrupting the original tetrahedral hydrogen bond structure, yielding distorted and heterogeneous network brushes.[38] Thus, the thinner hydration shell and unstable hydrogen bond system would form at the interface, where the

https://doi.org/10.1021/jacsau.2c00273
JACS Au 2022, 2, 1989−2000

lubrication layer (hydration shell) could be readily disrupted under the hydrodynamic force that produced a higher viscosity signified by the shear thickening behavior. The changes in the rheological properties with temperature could also be observed for the dense PNIPAM microgel suspension. The shear stress would be suppressed, and discontinuous shear thickening occurred at temperatures exceeding the LCST (red open triangles of Figure S11). The rheological profiles agreed with the prediction of recent molecular dynamics calculation and experiments.[35] The PO40-g-L.SEC displayed similar trend in the rheological behavior, where the shear thickening behavior was enhanced at high temperature. However, the conformational transition of $POEGMA_{188}$ brushes led to lower amounts of intermediate water contents as determined by the Raman measurements. Therefore, it could still form a stable hydrogen network between the PO40-g-L.SEC particles when compared with PN40-g-L.SEC at temperatures beyond the LCST, showing a smaller shear thickening enhancement (Figure S11B). In addition, additional rheological experiments were conducted on another type of polymer grafted pollen microparticles (Lotus), where the Lotus pollen possessed a similar size but with a different surface roughness (Figure S12). Both the PN40-g-L.SEC and PN40-g-Lotus particles displayed temperature-dependent viscosity variations. However, above the LCST, PN40-g-L.SEC possessed a higher shear thickening effect compared to PN40-g-Lotus.[39] This is attributed to the rougher PN40-g-L.SEC particle with an enhanced proportion of polymer−water interface, leading to a larger heterogeneity of the water structures due to the increased density of intermediate water.[40]

Moreover, surface free energy (γ_s) was affected by the rearrangement of hydrophilic/hydrophobic moieties, which is a key parameter to determine the wettability at the integrated air−liquid−solid interface. According to the Owens, Wendt, Rabel, and Kaelble (OWRK) theory,[41] the surface free energy consisted of both polar (γ_s^p) and dispersive components (γ_s^d), where the two polar -C=O, −NH groups, and apolar IP groups of PNIPAM contributed to γ_s^p and γ_s^d. Tables S3 and S4 provide a summary of the changes of surface free energy on PN-g-L.SEC and PO-g-L.SEC surfaces for the temperature at 20 and 40 °C. For the PN40-g-L.SEC surface, when the temperature was increased from 20 to 40 °C, γ_s^p decreased from 15.8 to 0.04 mJ m^{-2} and γ_s^d decreased from 39.5 to 32.6 mJ m^{-2}, suggesting that the surface switched from hydrophilic to hydrophobic and γ_s of 55.2 mJ m^{-2} decreased to 32.6 mJ m^{-2}. It can be concluded that the surface free energy contributed to the increased hydrophobicity of the surface owing to the polar/apolar component's conformational transition.

The temperature-dependent polymer conformational transition followed by the surrounding water structural transformation and surface free energy fluctuations further impacted the water structure at a macroscopic air−water-solid interface. When the grafting ratio increased to a critical value, the surface could display a switchable wettability behavior driven by temperature that amplified the interaction modes between the water molecules and the polymer chains. We selected two representative states of PN10-g-L.SEC and PO10-g-L.SEC surfaces to illustrate the surface superhydrophobicity transformation. Interestingly, for the PN10-L.SEC surface with an R_q of 2.32 μm, the surface displayed a superhydrophobic/superhydrophilic change with a CA of 3.1 ° at 20 °C and 154.3° at 40 °C (Figure 3B, Movie S1 and S2). The experimental results showed that the PN10-g-L.SEC (20 °C) surfaces with under-water superoleophobicity ($\theta_{ow} \sim 151.5°$) changed to $\theta_{ow} \sim 1.4°$ at 40 °C (Figure 2D). This demonstrated that the hydrophilic moieties of PNIPAM brushes on the PN10-g-L.SEC surface extended toward the water phase at 20 °C. Above the LCST (at 40 °C), the dehydration of hydrophobic groups induced the oil phase to displace the water phase on the surface. When the surface was prewetted by hexane, the IP groups interacted with hexane and repelled water driven by solvation (Figure 2D). Thus, the PN10-g-L.SEC surface exposed more hydrophilic groups at low temperatures, which transformed into the hydrophobic groups at higher temperature. A large amount of hydrophobic groups (2 methyl/per unit) endowed the surface with a low surface free energy of 29.3 mJ m^{-2}, and in combination with the hierarchical structure, it produced the superhydrophobic characteristic as indicated by the CA above the LCST. A similar thermal switching between superhydrophobicity and superhydrophilicity was observed for the PN20-g-L.SEC surface (Figure S14). Additionally, the PN10-g-L.SEC surface possessed a rapid transformation between superhydrophilicity and superhydrophobicity since a single cycle took only several minutes, changing between 2 and 150° on the PN10-g-L.SEC surface when the temperature cycled between 20 and 40 °C. This reversibility of the surface hydrophobicity remained after the sample was stored without special protection for more than three months, confirming that the polymer-L.SEC was robust and stable.

Additionally, we observed that the PO10-g-L.SEC surface displayed superhydrophilic characteristics in contrast to PN10-g-L.SEC. The interfacial behavior at air/ POm-g-L.SEC/water and the corresponding water affinity behavior were determined by the surface free energy of the hydrophobic MMA and hydrophilic OEG groups. Interestingly, the R_q was 2.25 μm for the PO10-g-L.SEC surfaces, where the CAs remained constant at 1° (20 °C) and 2° (40 °C), displaying superhydrophilicity without wettability transition (Figure 3E). Below the LCST (26.9 °C), the ether groups on PEG segments formed hydrogen bonds with water molecules. However, above the LCST, this balance was disrupted and the interaction between the side chain of $POEGMA_{188}$ and water decreased, resulting in the enhanced polymer−polymer interactions over polymer−water interactions. The $POEGMA_{188}$ chains collapsed into a globule conformation with the OEG chains/groups surrounding the hydrophobic MMA backbone yielding a less hydrophobic state (θ_i <90°), where the water repellent characteristic was less severe compared to PN10-g-L.SEC.[42] This phase transition behavior led to a more hydrophobic of $POEGMA_{188}$ globules above the LCST compared to the solvated chains at low temperature, with the overall characteristics being somewhat hydrophilic. Since the OEG segments resided on the outer surface of the collapsed chains with a higher surface free energy, hence, the water droplets deposited on the PO10-g-L.SEC surface would spread with a low CA of 2°. These results confirmed the intrinsic hydrophilic characteristic of the polymer chain conformation together with the hierarchical structure that controlled the surface wettability. To conclude, the thermally responsive switching between superhydrophobic and superhydrophilic states of PNm-g-L.SEC surfaces (m ∼ 10, 20) was observed due to the reduced low surface free energy caused by the hydrophobic IP moieties orientation at air/solid/water interface. In contrast, POm-g-L.SEC surfaces (m ∼ 10, 20) possessed a higher surface free energy due to the hydrophilic PEG segments being exposed to the interface resulting in a non-switchable wettability phenomenon.

https://doi.org/10.1021/jacsau.2c00273
JACS Au 2022, 2, 1989−2000

To further confirm the mechanism of hydrophobic enhancement induced by the surface roughness and the interfacial water structure transformation, we imaged the 3D contact interface between the liquid droplet and the PN10-g-L.SEC surface at 20 and 40 °C via confocal laser microscopy. Below the LCST, the stable and ordered hydrogen bond network promoted the wetting of the microparticle surface by water molecules that also occupied the gap between the microparticles generating superhydrophilic domains as indicated in Figure S15A. The green dots (fluorescence-stained) persisted from the base substrate to the outer surface, demonstrating the fully wetted state. Above the LCST, the droplet contacts with the PN10-g-L.SEC surface revealed that the liquid baseline was suspended between particles, indicating a non-wetted state (Figure S15B). This observation further demonstrates that the more disordered water structure (intermediate water) caused by the polymer chain transition induced a weaker binding interaction, resulting in a lower tendency to wet the surface. Thus, the liquid would not penetrate the air-pockets to fill the surface resulting in the observed superhydrophobic character of the substrate.

The molecular structure and chemical composition of PNIPAM and $POEGMA_{188}$ impacted the interaction between water molecules and polymer brushes, which controlled the hydrophobicity transition characteristics of the surface. Preferential exposure of the hydrophobic or hydrophilic moieties of the polymer-L.SEC altered the interfacial characteristics of the surrounding solvents (water or oil) and the surface, which could be used to manipulate the macroscopic wettability. Thus, these pollen-based thermo-responsive surfaces offer a novel design strategy to control the surface wettability transformation and exploit for various on-demand applications, such as emulsion separation. The switchable oil and water repellency driven by temperature can be conducted by alternately prewetting with water and oil, which gives the separation membrane the versatility to handle oil−water mixtures (Figure S16).

CONCLUSIONS

In summary, we studied the temperature-dependent interfacial properties on thermo-responsive surfaces. Specifically, we investigated the assemblies of microparticles grafted with two types of LCST polymers, PNIPAM and $POEGMA_{188}$, and correlated the interfacial water structure variation at a multiple length scale with the wettability transition of the integrated surface (formed by the self-assembly of microparticles), as revealed by Raman measurements, supplementary rheology experiments, and confocal microscopy. From the analysis at the nanoscale and macroscale length scales, we concluded that the increased intermediate water (decreased bonded water structure) with combined surface roughness resulted in the enhanced hydrophobicity. This surface design strategy provides information that correlates the molecular-level conformational transition with the macroscopic surface wettability. Moreover, the knowledge and fundamental understanding derived from this study demonstrate the potential application of PNIPAM and $POEGMA_{188}$ by controlling the interfacial water structure at the solid−liquid interface in other systems, such as biobased responsive surfaces.[43]

ASSOCIATED CONTENT

Supporting Information

The Supporting Information is available free of charge at https://pubs.acs.org/doi/10.1021/jacsau.2c00273.

Extraction of L.SEC particles, preparation of the thermo-responsive L.SEC based surface, contact angle measurements, LCST behaviors, surface topography, interface energy calculation, surface free energy and emulsion separation application (Figures S1−S15, Tables S1−S4) (PDF)

Wettability transformation of PN10-g-L.SEC driven by temperature (Movie S1) (MP4)

Wettability transformation of PN10-g-L.SEC driven by temperature (Movie S2) (MP4)

AUTHOR INFORMATION

Corresponding Author

Kam Chiu Tam − *Department of Chemical Engineering, Waterloo Institute for Nanotechnology, University of Waterloo, Waterloo, Ontario N2L 3G1, Canada;* orcid.org/0000-0002-7603-5635; Email: mkctam@uwaterloo.ca

Authors

Yi Wang − *Department of Chemical Engineering, Waterloo Institute for Nanotechnology, University of Waterloo, Waterloo, Ontario N2L 3G1, Canada*

Weinan Zhao − *Department of Chemical Engineering, Waterloo Institute for Nanotechnology, University of Waterloo, Waterloo, Ontario N2L 3G1, Canada*

Mei Han − *Department of Chemical Engineering, Waterloo Institute for Nanotechnology, University of Waterloo, Waterloo, Ontario N2L 3G1, Canada*

Jiaxin Xu − *Department of Chemical Engineering, Waterloo Institute for Nanotechnology, University of Waterloo, Waterloo, Ontario N2L 3G1, Canada*

Xiaoming Zhou − *Department of Chemical Engineering, Waterloo Institute for Nanotechnology, University of Waterloo, Waterloo, Ontario N2L 3G1, Canada*

Wesley Luu − *Department of Chemical Engineering, Waterloo Institute for Nanotechnology, University of Waterloo, Waterloo, Ontario N2L 3G1, Canada*

Lian Han − *Department of Chemical Engineering, Waterloo Institute for Nanotechnology, University of Waterloo, Waterloo, Ontario N2L 3G1, Canada*

Complete contact information is available at: https://pubs.acs.org/10.1021/jacsau.2c00273

Author Contributions

‡Y.W. and W.Z. contributed equally.

Author Contributions

CRediT: **Yi Wang** conceptualization, data curation, formal analysis, investigation, methodology, writing-original draft; **Weinan Zhao** conceptualization, data curation, formal analysis, investigation, methodology, writing-original draft; **Mei Han** data curation, investigation, methodology; **Jiaxin Xu** investigation, methodology; **Xiaoming Zhou** investigation, methodology; **Wesley Luu** investigation, methodology; **Lian Han** investigation, methodology; **Kam Chiu Tam** conceptualization, formal analysis, project administration, resources, supervision, validation, writing-review & editing.

https://doi.org/10.1021/jacsau.2c00273
JACS Au 2022, 2, 1989−2000

Notes

The authors declare no competing financial interest.

■ ACKNOWLEDGMENTS

K.C.T. wishes to acknowledge the financial support from NSERC and CFI Canada. Y.W. is grateful to the support of China Scholarship Council (CSC).

■ REFERENCES

(1) Russell, T. P. Surface-Responsive Materials. *Science* **2002**, *297*, 964−967.
(2) Dubovik, A. S.; Kuznetsov, D. V.; Grinberg, N. V.; Grosberg, A. Y.; Tanaka, T. Studies of the Thermal Volume Transition of Poly(N-isopropylacrylamide) Hydrogels by High-Sensitivity Differential Scanning Microcalorimetry. 2. Thermodynamic Functions. *Macromolecules* **2000**, *33*, 8685−8692.
(3) Monosmith, W. B.; Walrafen, G. E. Temperature dependence of the Raman OH-stretching overtone from liquid water. *J. Chem. Phys.* **1984**, *81*, 669−674.
(4) Liu, M.; Leroux, J.-C.; Gauthier, M. A. Conformation−function relationships for the comb-shaped polymer pOEGMA. *Prog. Polym. Sci.* **2015**, *48*, 111−121.
(5) Okada, K.; Miura, Y.; Chiya, T.; Tokudome, Y.; Takahashi, M. Thermo-responsive wettability via surface roughness change on polymer-coated titanate nanorod brushes toward fast and multi-directional droplet transport. *RSC Adv.* **2020**, *10*, 28032−28036.
(6) Zhao, Z.; Ning, Y.; Jin, X.; Ben, S.; Zha, J.; Su, B.; Tian, D.; Liu, K.; Jiang, L. Molecular-Structure-Induced Under-Liquid Dual Superlyophobic Surfaces. *ACS Nano* **2020**, *14*, 14869−14877.
(7) Potroz, M. G.; Mundargi, R. C.; Gillissen, J. J.; Tan, E.-L.; Meker, S.; Park, J. H.; Jung, H.; Park, S.; Cho, D.; Bang, S.-I.; Cho, N.-J. Plant-Based Hollow Microcapsules for Oral Delivery Applications: Toward Optimized Loading and Controlled Release. *Adv. Funct. Mater.* **2017**, *27*, 1700270.
(8) Zhao, Z.; Hwang, Y.; Yang, Y.; Fan, T.; Song, J.; Suresh, S.; Cho, N.-J. Actuation and locomotion driven by moisture in paper made with natural pollen. *Proc. Natl. Acad. Sci. U. S. A.* **2020**, *117*, 8711−8718.
(9) Hou, X.; Hu, Y.; Grinthal, A.; Khan, M.; Aizenberg, J. Liquid-based gating mechanism with tunable multiphase selectivity and antifouling behaviour. *Nature* **2015**, *519*, 70−73.
(10) Chen, C.; Kuang, Y.; Hu, L. Challenges and opportunities for solar evaporation. *Joule* **2019**, *3*, 683−718.
(11) Zhao, F.; Zhou, X.; Shi, Y.; Qian, X.; Alexander, M.; Zhao, X.; Mendez, S.; Yang, R.; Qu, L.; Yu, G. Highly efficient solar vapour generation via hierarchically nanostructured gels. *Nat. Nanotechnol.* **2018**, *13*, 489−495.
(12) Xu, X.; Ozden, S.; Bizmark, N.; Arnold, C. B.; Datta, S. S.; Priestley, R. D. A Bioinspired Elastic Hydrogel for Solar-Driven Water Purification. *Adv. Mater.* **2021**, *33*, 2007833.
(13) Qing, G.; Zhao, X.; Gong, N.; Chen, J.; Li, X.; Gan, Y.; Wang, Y.; Zhang, Z.; Zhang, Y.; Guo, W.; Luo, Y.; Liang, X.-J. Thermo-responsive triple-function nanotransporter for efficient chemo-photothermal therapy of multidrug-resistant bacterial infection. *Nat. Commun.* **2019**, *10*, 4336.
(14) Zhao, Z.; Kumar, J.; Hwang, Y.; Deng, J.; Ibrahim Mohammed Shahrudin, B.; Huang, C.; Suresh, S.; Cho, N.-J. Digital printing of shape-morphing natural materials. *Proc. Natl. Acad. Sci. U. S. A.* **2021**, *118*, e2113715118.
(15) Jiao, Y.; Tibbits, A.; Gillman, A.; Hsiao, M.-S.; Buskohl, P.; Drummy, L. F.; Vaia, R. A. Deformation Behavior of Polystyrene-Grafted Nanoparticle Assemblies with Low Grafting Density. *Macromolecules* **2018**, *51*, 7257−7265.
(16) Sun, B.; Lin, Y.; Wu, P.; Siesler, H. W. A FTIR and 2D-IR Spectroscopic Study on the Microdynamics Phase Separation Mechanism of the Poly(N-isopropylacrylamide) Aqueous Solution. *Macromolecules* **2008**, *41*, 1512−1520.
(17) Cho, E. C.; Lee, J.; Cho, K. Role of Bound Water and Hydrophobic Interaction in Phase Transition of Poly(N-isopropylacrylamide) Aqueous Solution. *Macromolecules* **2003**, *36*, 9929−9934.
(18) Harrison, R. H.; Steele, J. A. M.; Chapman, R.; Gormley, A. J.; Chow, L. W.; Mahat, M. M.; Podhorska, L.; Palgrave, R. G.; Payne, D. J.; Hettiaratchy, S. P.; Dunlop, I. E.; Stevens, M. M. Modular and Versatile Spatial Functionalization of Tissue Engineering Scaffolds through Fiber-Initiated Controlled Radical Polymerization. *Adv. Funct. Mater.* **2015**, *25*, 5748−5757.
(19) Yang, H.; Zhu, H.; Hendrix, M. M. R. M.; Lousberg, N. J. H. G. M.; de With, G.; Esteves, A. C. C.; Xin, J. H. Temperature-Triggered Collection and Release of Water from Fogs by a Sponge-Like Cotton Fabric. *Adv. Mater.* **2013**, *25*, 1150−1154.
(20) Davis, J. G.; Gierszal, K. P.; Wang, P.; Ben-Amotz, D. Water structural transformation at molecular hydrophobic interfaces. *Nature* **2012**, *491*, 582−585.
(21) Kolberg, A.; Wenzel, C.; Hackenstrass, K.; Schwarzl, R.; Rüttiger, C.; Hugel, T.; Gallei, M.; Netz, R. R.; Balzer, B. N. Opposing Temperature Dependence of the Stretching Response of Single PEG and PNiPAM Polymers. *J. Am. Chem. Soc.* **2019**, *141*, 11603−11613.
(22) Wang, Y.; Zhao, W.; Han, M.; Guan, L.; Han, L.; Hemraj, A.; Tam, K. C. Sustainable Superhydrophobic Surface with Tunable Nanoscale Hydrophilicity for Water Harvesting Applications. *Angew. Chem., Int. Ed.* **2022**, *61*, No. e202115238.
(23) Rey, M.; Law, A. D.; Buzza, D. M. A.; Vogel, N. Anisotropic Self-Assembly from Isotropic Colloidal Building Blocks. *J. Am. Chem. Soc.* **2017**, *139*, 17464−17473.
(24) Guzmán, E.; Martínez-Pedrero, F.; Calero, C.; Maestro, A.; Ortega, F.; Rubio, R. G. A broad perspective to particle-laden fluid interfaces systems: from chemically homogeneous particles to active colloids. *Adv. Colloid Interface Sci.* **2022**, *302*, 102620.
(25) Lutz, J.-F.; Akdemir, Ö.; Hoth, A. Point by Point Comparison of Two Thermosensitive Polymers Exhibiting a Similar LCST: Is the Age of Poly(NIPAM) Over? *J. Am. Chem. Soc.* **2006**, *128*, 13046−13047.
(26) Liu, M.; Wang, S.; Jiang, L. Nature-inspired superwettability systems. *Nat. Rev. Mater.* **2017**, *2*, 17036.
(27) Wang, D.; Sun, Q.; Hokkanen, M. J.; Zhang, C.; Lin, F.-Y.; Liu, Q.; Zhu, S.-P.; Zhou, T.; Chang, Q.; He, B.; Zhou, Q.; Chen, L.; Wang, Z.; Ras, R. H. A.; Deng, X. Design of robust superhydrophobic surfaces. *Nature* **2020**, *582*, 55−59.
(28) Sun, T.; Wang, G.; Feng, L.; Liu, B.; Ma, Y.; Jiang, L.; Zhu, D. Reversible Switching between Superhydrophilicity and Superhydrophobicity. *Angew. Chem., Int. Ed.* **2004**, *43*, 357−360.
(29) Wong, T.-S.; Kang, S. H.; Tang, S. K. Y.; Smythe, E. J.; Hatton, B. D.; Grinthal, A.; Aizenberg, J. Bioinspired self-repairing slippery surfaces with pressure-stable omniphobicity. *Nature* **2011**, *477*, 443−447.
(30) Wang, Y.; Di, J.; Wang, L.; Li, X.; Wang, N.; Wang, B.; Tian, Y.; Jiang, L.; Yu, J. Infused-liquid-switchable porous nanofibrous membranes for multiphase liquid separation. *Nat. Commun.* **2017**, *8*, 575.
(31) Smith, J. D.; Cappa, C. D.; Drisdell, W. S.; Cohen, R. C.; Saykally, R. J. Raman Thermometry Measurements of Free Evaporation from Liquid Water Droplets. *J. Am. Chem. Soc.* **2006**, *128*, 12892−12898.
(32) Li, C.; Cao, S.; Lutzki, J.; Yang, J.; Konegger, T.; Kleitz, F.; Thomas, A. A Covalent Organic Framework/Graphene Dual-Region Hydrogel for Enhanced Solar-Driven Water Generation. *J. Am. Chem. Soc.* **2022**, *144*, 3083−3090.
(33) Giovambattista, N.; Debenedetti Pablo, G.; Rossky Peter, J. Enhanced surface hydrophobicity by coupling of surface polarity and topography. *Proc. Natl. Acad. Sci. U. S. A.* **2009**, *106*, 15181−15185.
(34) Miyazaki, M.; Fujii, A.; Ebata, T.; Mikami, N. Infrared spectroscopic evidence for protonated water clusters forming nanoscale cages. *Science* **2004**, *304*, 1134−1137.
(35) Hsu, C.-P.; Mandal, J.; Ramakrishna, S. N.; Spencer, N. D.; Isa, L. Exploring the roles of roughness, friction and adhesion in discontinuous shear thickening by means of thermo-responsive particles. *Nat. Commun.* **2021**, *12*, 1477.

https://doi.org/10.1021/jacsau.2c00273
JACS Au 2022, 2, 1989−2000

(36) Chen, L.; He, X.; Liu, H.; Qian, L.; Kim, S. H. Water Adsorption on Hydrophilic and Hydrophobic Surfaces of Silicon. *J. Phys. Chem. C* **2018**, *122*, 11385−11391.
(37) Cheng, X.; McCoy Jonathan, H.; Israelachvili Jacob, N.; Cohen, I. Imaging the Microscopic Structure of Shear Thinning and Thickening Colloidal Suspensions. *Science* **2011**, *333*, 1276−1279.
(38) Shin, S.; Willard, A. P. Water's Interfacial Hydrogen Bonding Structure Reveals the Effective Strength of Surface−Water Interactions. *J. Phys. Chem. B* **2018**, *122*, 6781−6789.
(39) James, N. M.; Han, E.; de la Cruz, R. A. L.; Jureller, J.; Jaeger, H. M. Interparticle hydrogen bonding can elicit shear jamming in dense suspensions. *Nat. Mater.* **2018**, *17*, 965−970.
(40) Guzmán, E.; Tajuelo, J.; Pastor, J. M.; Rubio, M. Á.; Ortega, F.; Rubio, R. G. Shear rheology of fluid interfaces: Closing the gap between macro- and micro-rheology. *Curr. Opin. Colloid Interface Sci.* **2018**, *37*, 33−48.
(41) Owens, D. K.; Wendt, R. C. Estimation of the surface free energy of polymers. *J. Appl. Polym. Sci.* **1969**, *13*, 1741−1747.
(42) Tang, J.; Berry, R. M.; Tam, K. C. Stimuli-Responsive Cellulose Nanocrystals for Surfactant-Free Oil Harvesting. *Biomacromolecules* **2016**, *17*, 1748−1756.
(43) Dhyani, A.; Wang, J.; Halvey Alex, K.; Macdonald, B.; Mehta, G.; Tuteja, A. Design and applications of surfaces that control the accretion of matter. *Science* **2021**, *373*, eaba5010.

https://doi.org/10.1021/jacsau.2c00273
JACS Au 2022, 2, 1989−2000